Reliability-based Retrofit Assessment of Coastal Bridges Subjected to Wave Forces using 3D Numerical modeling and Machine Learning

Deming Zhu[1], and You Dong[2, *]

Abstract

This paper proposes a comprehensive analysis framework, combining three-dimensional (3D) numerical model and machine learning, to investigate probabilistic performance of retrofit actions on coastal bridges subjected to extreme wave forces. Specifically, a 3D Computational Fluid Dynamics (CFD) model is developed to calculate extreme wave load on the bridge superstructure, which could provide more accurate results as compared with traditional two-dimensional (2D) model. The established 3D model is validated by laboratory experiments. The characteristics of wave forces are parametrically investigated, and an Artificial Neural Network (ANN) model is utilized to quantify the loading effects with multiple surge and wave parameters. Such numerical-based ANN model could predict wave forces under variable scenarios accurately, and significantly reduce the high computational cost of the 3D numerical model. Based on the numerical and machine learning results, the bridge fragility curve is derived by considering uncertainties associated with structural demand, capacity, and hurricane hazard. Long-term failure risk is assessed under different climate change scenarios. Furthermore, different retrofit methods to improve structural performance and reduce failure risk are examined according to the proposed framework, including inserting air venting hole, enhancing connection strength, and elevating bridge structure. The proposed framework could facilitate the optimal and robust design and maintenance of coastal infrastructures under hurricane effects in a long-term time interval.

Keywords: Coastal bridge; 3D CFD model; Retrofit; Artificial Neural Network; Climate change; Probabilistic fragility model.

---

[1] Ph.D. student, The Hong Kong Polytechnic University, Department of Civil and Environmental Engineering, Hung Hom, Hong Kong, China, deming.zhu@connect.polyu.hk.

[2] Assistant Professor of Structural Engineering, The Hong Kong Polytechnic University, Department of Civil and Environmental Engineering, Hung Hom, Hong Kong, China, you.dong@polyu.edu.hk. *Corresponding Author.

1. Introduction

Due to the climate change scenarios (*e.g.*, the increasing sea level rise and amplification of cyclone intensity), the extreme waves could approach the coastal bridges and lead to severe damage, especially for the low-lying simply supported bridges. For instance, the hurricane Ivan (2004) and Katrina (2005) destroyed a number of coastal bridges along the Gulf Coast of Mexico (Huang & Xiao 2009; Okeil & Cai 2008). Since then, wave load calculation for bridge under hurricane induced surge, wind and wave has attracted increasing attention. Damaged bridges not only cause direct financial loss, but also affect transportation and rescue problem, threatening public safety. Vulnerability and reliability analysis for existing bridges, and identification of appropriate retrofit measure could reduce bridge failure risk as well as maintenance cost (Dong & Frangopol, 2016; Li et al., 2020; Qin, 2018). Thus, a systematic analysis of coastal bridge performance under hurricane waves, and evaluation of retrofit methods are of vital importance.

The bridge failure mode and associated capacity and demand should be first identified, which requires a deep exploration on bridge performance under hurricane-induced wave and surge loads. Douglass et al., (2004); Padgett et al., (2008); and Robertson et al., (2007) conducted field surveys on the damaged coastal bridges during Hurricane Ivan and Hurricane Katrina, and accordingly, one of the major failure modes is deck unseating (Akiyama et al. 2012; Ataei & Padgett 2013; BRICKER 2011). The combination of hydrodynamic and hydrostatic forces, as well as effects of trapped air, could overcome the weight of the superstructure (Hayatdavoodi et al. 2014a; Hayatdavoodi & Ertekin 2016). The wave-deck interaction has aroused increasing concern in last decade, and more studies are required considering the complicated hydrodynamic problem. For instance, Bradner et al., (2011) conducted a 1:5 scale experiment to measure the wave loads on the bridge superstructure, observing a second-order relationship between force and wave height. Guo et al., (2015) experimentally measured wave force on a bridge deck under regular waves and compared with analytical results. Considering the high expense of large-scale experiment, numerical studies based on two-dimensional (2D) model have also been well adopted (Jin & Meng, 2011; Seiffert et al., 2014; Xiao et al., 2010). However, Xu et al., (2016) conducted numerical research of solitary wave forces, and concluded that a 2D model may not fully capture some features and a three-dimensional (3D) model was recommended for future studies. Bozorgnia & Lee, (2012) and Motley et al., (2016) also pointed out that simplification by using 2D model could lead to errors, and 3D model should be studied for more reliable results. There is growing focus on the utilization of spatial (3D) model on the structural reliability analysis and risk management (Qin 2012; Qin & Faber 2012). Therefore, this study utilizes a 3D Computational Fluid Dynamics (CFD) model to simulate the wave-deck interaction and to compute the maximum wave loads. Such method was compared and validated by experimental measurements (Zhu & Dong 2020). Also, discussion and comparisons of the differences between 2D and 3D computational results are presented in this paper. In this study, the solitary wave model is adopted to simulate extreme hurricane waves for its stable form and advantages of parametric study (Veritas 2000). Given a preliminary understanding on structural responses, other types of waves (e.g., periodic wave and cnoidal waves) will be investigated in future studies.

Since bridge damages can result in large economic and safety consequences, retrofit measures applied to existing bridges are important for coastal infrastructure management (Mondoro et al. 2017). Three retrofit methods investigated in this study include elevating bridge structure, enhancing connection strength, and inserting air venting holes. Elevation of the bridge superstructure for larger clearance is one of the most effective methods, since the surge and wave load depends significantly on the relative distance from the water level to the bridge deck (Xu & Cai 2017). Based on investigations on wave forces on coastal bridge decks, elevating bridge structures to reduce failure risk was highlighted (Padgett et al., 2008; Xu et al., 2017). Such method has been adopted to prevent surge and flooding risk in New York City region for coastal infrastructures (NYCDEP 2008; Rosenzweig et al. 2011).

In addition, tie-down, restrainer, and anchorage bar, among others, may be added to bridge to provide additional connection between the substructure and superstructure (Zheng et al. 2018; Zheng & Dong 2019). These devices increase the capacity to resist upward and transverse movement subjected to surge and wave forces during hurricanes (Robertson et al. 2007).

Robertson et al., (2011) conducted survey on the damaged bridges during Hurricane Katrina, and found the connections were inadequately designed. Lehrman et al., (2012) examined structural performance of three commonly used connections: headed studs, through bolts, and clip bolts under different loading conditions. It was concluded that none of the anchorages could withstand the extreme wave forces, and combination of these connections is necessary. Thus, enhancing connection strength as a potential adaptation method is investigated in this study.

Furthermore, inserting holes in the superstructure to allow entrapped air beneath the deck to flow out can reduce total vertical force (AASHTO 2008; Sawyer 2008). It has been proven that the trapped air between girders and deck could significantly increase vertical wave loads (Azadbakht & Yim 2016; Bricker & Nakayama 2014; Istrati & Buckle 2019; Matemu et al. 2020), and there were several studies focusing on the countermeasure of inserting air venting holes (Cuomo et al., 2009; Hayatdavoodi et al., 2014b; Xu et al., 2017). However, due to the complex wave-air-deck interaction, there are deviations when converting experimental-scale results to prototype-scale results (Seiffert, 2014). Detailed investigations targeting on specific cases are recommended for practical engineering problem (AASHTO 2008), and this aspect is conducted in this study.

Nowadays, the climate change has caused an increasing threat to coastal infrastructures. There has been growing evidence that the climate change could affect both the frequency and intensity of hurricane events (Bender et al. 2010; Elsner et al. 2008). Knutson et al., (2010) assessed the hurricane speed may increase by 20% around the world in the 21st century. Australian Greenhouse office also claimed that wind speed would increase by 5-10% by year 2070. Long-term performance of coastal bridges considering climate change issues has aroused widespread concern within the hazard management process. For example, Biondini & Frangopol, (2016), Dong & Frangopol, (2017), and Guo & Chen, (2016) focused on life-cycle cost of infrastructure systems and highlighted the necessity of applying mitigation strategies to deal with climate change effects. Moftakhari et al., (2017) assessed the increase in failure probabilities caused by compounding effects of sea level rise and flooding. Khelifa et al., (2013) estimated that the long-term loss of bridge infrastructures would increase 15% under climate change scenarios. Thus, adaptation methods of coastal bridges are necessary considering the intensifying climate change scenarios.

Although there existed several studies on hydraulic loads on coastal bridges caused by surge and waves, it still lacks a systematic investigation on the structural reliability and effects of relative retrofit measures on structural long-term performance based on 3D numerical model. To address this issue, the first objective of this study is to better investigate the vulnerability and reliability of coastal bridges subjected to extreme waves. The second objective is to examine the effects of different retrofit measures in reducing the long-term bridge failure risk. The considered retrofit actions include inserting air venting hole, enhancing connection strength, and elevating bridge structure. To this end, this study proposes a systematic framework to investigate the vulnerability and reliability of coastal bridges under different retrofit actions. An experimental validated 3D numerical model is established to investigate the complex wave-structure interaction, calculating more accurate wave force as compared with traditional 2D model. Differences between 2D and 3D are presented and discussed. Then, the characteristics of the wave forces are parametrically investigated and modeled by the Artificial Neural Network (ANN), which provides a prediction method for wave forces under various conditions and significantly reduces computational cost. Subsequently, bridge fragility curves are derived for different hurricane scenarios by considering the uncertainties associated with structural capacity and demand. The long-term bridge failure risk is assessed by considering the climate change effects. Based on the proposed framework, different retrofit methods are examined and compared, including inserting air venting holes, enhancing connection strength, and elevating bridge structure. The remainder of the paper are organized as follows. The 3D numerical investigations on wave-structure interaction and ANN modeling are presented in section 2. The bridge reliability and risk analysis are introduced in section 3. Evaluation and comparison of different retrofit methods are shown in section 4. Finally, conclusions are drawn, and future work is highlighted in section 5.

2. Investigation on the wave force using 3D CFD model

Due to the complex wave-structure interaction and high expense of large-scale experiment, numerical simulation is a common method to assess the wave induced force on the bridge. However, results from traditional 2D model could deviate from the real values due to spatial limitation of the numerical domain (Zhu & Dong 2020). The complicated hydrodynamic problem, including the wave deformation, trapped air between girders and deck, and wave overtopping phenomenon, could not be well simulated in a 2D model. A more sufficient model (*i.e.*, 3D model) is required for better results. Recognizing this, this study establishes a 3D Computational Fluid Dynamics (CFD) model with *ANSYS Fluent*. The relative model setups, numerical results, experimental validation, comparisons between 2D and 3D models, and data processing and discussion are presented in this section.

2.1 3D CFD modeling and boundary conditions

A typical I-10 simply supported bridge located in the south-east coastline of Florida, USA is selected as shown in Fig. 1 (a). The type of bridges built over Escambia Bay (Florida) were severely damaged during Hurricane Ivan (2004). Detailed reconnaissance report could be found in Douglass et al., (2004). For the investigated bridge model, the span is 15.85 m long, and has six I-shaped girders evenly distributed along the deck. The deck width is 9.6 m, and the total height, as the sum of girder height and deck thickness, is 1.44 m. 4 pairs of flip-bolt connections (a total of 8) are used to connect the bridge superstructure and substructure at seaward and landward bearings (Yuan et al. 2018).

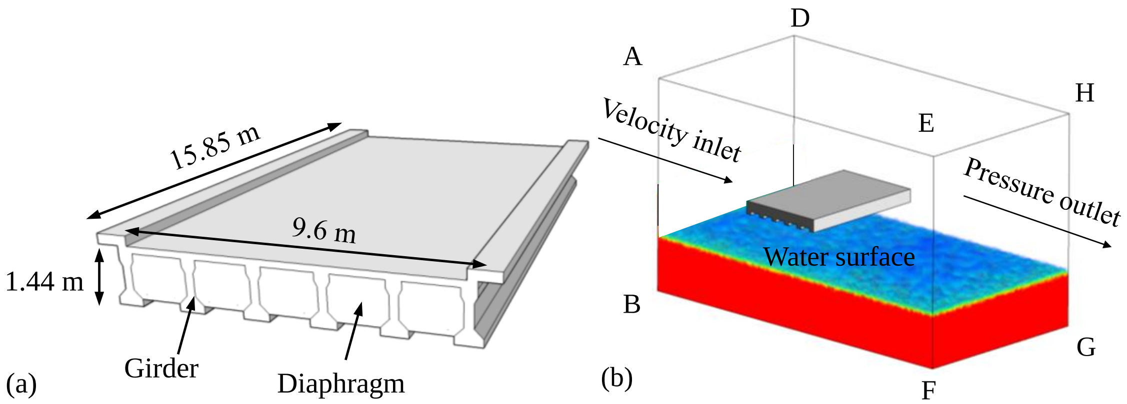

Fig. 1 (a) Investigated bridge model and (b) 3D CFD model and boundary conditions

The established 3D CFD domain and boundary conditions are shown in Fig. 1 (b). The I-shaped girders are simplified as rectangular to increase the computational efficiency (Huang & Xiao 2009). The initial water depth is set as 10 m, and initial clearance is 4 m. The wave is generated at the velocity inlet plane ABCD by using User Defined Functions (UDF) and flows towards the pressure outlet plane EFGH. Plane ADHE is set as pressure outlet with one atmosphere (*i.e.*, 101, 325 kPa). Other planes are set as stationary wall. Note that Fig. 1 (b) only presents part of the computational domain, and there is another 100 m long domain between the outlet plane and bridge model to minimize the wave reflection effects. The meshes of this part are relatively coarsen, which could both increase the calculation speed and reduce wave reflection.

In this study, the solitary wave model (Sarpkaya & Isaacson 1981) is employed to simulate the extreme waves. A soliton could maintain a relatively stable waveform within processing, which is beneficial for parametric study on wave force and experimental validation for the numerical model. In addition, the extreme impact from a soliton could highly exceed the deck weight, and thus this model has been often adopted in previous research on tsunamis and hurricanes (Madsen et al. 2008; MUNK 1949; Zhang et al. 2015). The dimensional quantities to describe the wave profile are

$$\eta(x,t) = H \operatorname{sech}^2 \sqrt{\frac{3}{4}\frac{H}{D^3}}(x-ct) \tag{1}$$

$$c = \sqrt{g(D+H)} \tag{2}$$

where η = free surface elevation above still water level; x = distance from the origin; t = time; D = water depth; H = wave height; c = wave celerity; and g = gravitational acceleration. The wave particle velocities u (in x direction, same as the wave flow) and v (in y direction, vertical to the ground) are determined as (Sarpkaya & Isaacson 1981)

$$\frac{u}{\sqrt{gD}} = \varepsilon \operatorname{sech}^2 q + \varepsilon^2 \operatorname{sech}^2 q \left\{ \frac{1}{4} - \operatorname{sech}^2 q - \frac{3}{4}\left(\frac{s}{D}\right)^2 \left(2 - 3\operatorname{sech}^2 q\right) \right\} \tag{3}$$

$$\frac{v}{\sqrt{gD}} = \varepsilon\sqrt{3\varepsilon}\left(\frac{s}{D}\right)\operatorname{sech}^2 q \tanh q \left\{1-\varepsilon\left[\frac{3}{8}+2\operatorname{sech}^2 q+\frac{1}{2}\left(\frac{s}{D}\right)^2\left(1-3\operatorname{sech}^2 q\right)\right]\right\} \tag{4}$$

$$q = \frac{\sqrt{3\varepsilon}}{2D}\left(1-\frac{5}{8}\varepsilon\right)\left(x-ct\right) \tag{5}$$

where $\varepsilon = H / D$; $s = y + D$; and y = the distance from the still water level to the wave crest, which is negative if the free surface is lower than the initial water level.

In the simulation process, the volume of fluid method (VOF) is used to predict the changing dynamic free surface. Air is set as phase-1, and water-liquid is set as phase-2. The water and air are assumed as incompressible flow. The shear stress transport (SST k-ω) model is used to capture the turbulent characters of the wave-deck interaction. In the numerical domain, tetrahedron mesh is utilized around the bridge model to fit its irregular shape. The mesh sizes are examined by performing mesh sensitivity analysis to satisfy the Courant Number (Robertsson & Blanch 2020). After several calculations and comparisons, the tetrahedron mesh size is determined as 0.6 m and the fixed time step is 0.01 s. The corresponding Courant Numbers of the investigated cases are around 1/3.

2.2 Experimental setups and validation

The established 3D CFD model was validated by laboratory experiment. A 1:30 scale experiment designed according to Froude similitude (Steffler 1999) was conducted at the Hydraulics Laboratory of the Hong Kong Polytechnic University as shown in Fig. 2 (a). Wave induced forces on the bridge model under different wave conditions were measured and compared with numerical results, proving the accuracy of the 3D CFD model.

The 1:30 scale bridge model was made of acrylic board, 0.52 m in length and 0.32 m in width. The laboratory experiment was conducted in a 30 m long wave channel. The wave channel is 1.5 m in width and 2 m in height. A piston type wave maker controlled by DHI (Danish Hydraulic Institute) system was set at one end of the channel to generate waves. A slope and several floating foam blocks were set on the other end to minimize wave reflections. Capacitive wave gauges were utilized to measure the changing water surface, and a multi-axis load cell was equipped to measure the wave loads on the deck at a frequency of 100 Hz (as Fig. 2 (b)). Instrument calibration is performed for the load cell in x, y, and z directions, respectively. A schematic diagram of the experimental setup is shown in Fig. 2 (c). This study mainly focuses on vulnerability analyses of coastal bridges and retrofit measures, and more details of experimental setups and model validation could be found in Zhu & Dong, (2020).

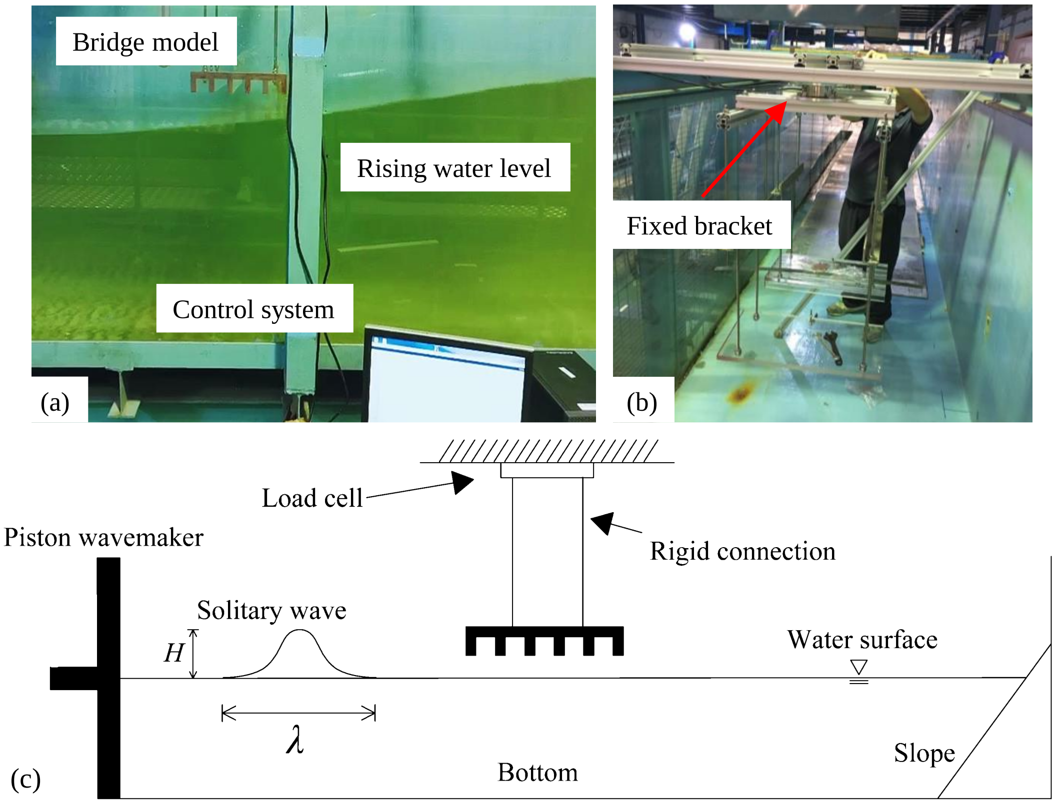

Fig. 2 (a) Photo of the bridge model during the test; (b) photo of installation of experimental facilities; and (c) schematic diagram of the experimental setup

2.3 Comparisons of 2D and 3D CFD models

Comparisons of the simulated wave progressing in the 2D and 3D CFD models are presented in Fig. 3, in which the interactions of water and air phases are represented by different colors (1 for water phase and 0 for air phase based on the VOF method). Apparently, the 2D model could not simulate the wave and air flow in the longitudinal direction (z axis), thus, the air is fully trapped between girders and deck, as indicated in Fig. 3 (a). In contrast, the 3D model contains more structural details including girders and diaphragms, and successfully simulates the wave-air interaction between deck and water surface, as shown in Fig. 3 (b). More details could be found in the top view of the 3D model as Fig. 3 (c). Thus, a 3D model could provide more reliable results as compared with a 2D model.

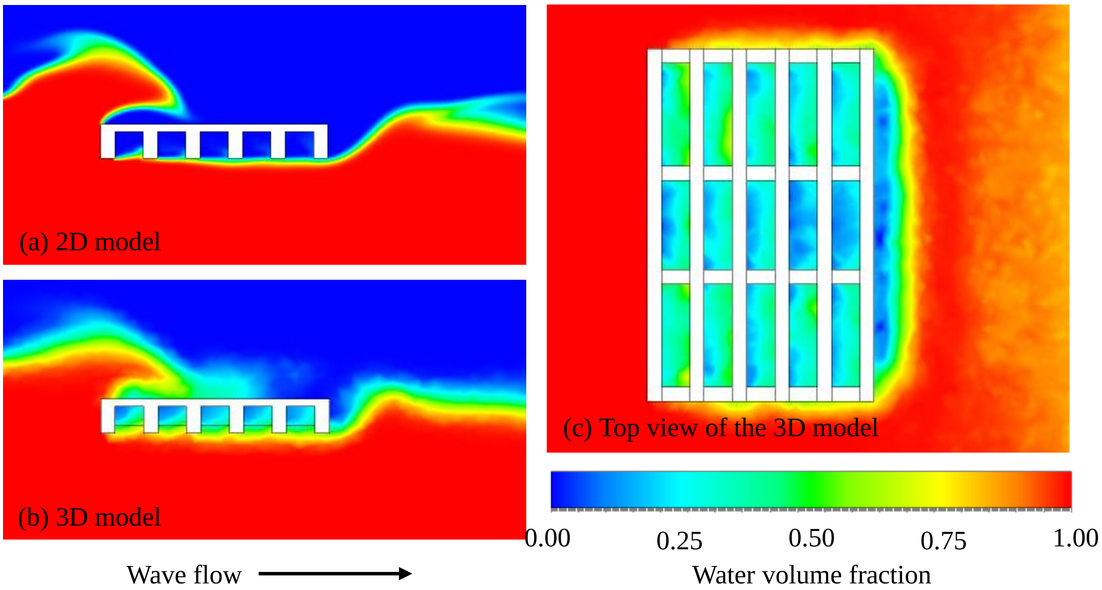

Fig. 3 Comparisons of wave profiles in the 2D and 3D models

In addition, comparisons of maximum vertical and horizontal wave forces (F_v and F_h) calculated from 2D and 3D CFD models are presented in Fig. 4. The water depth of the illustrated cases is 12 m, and the associated clearance Z_c is 2 m. Note that wave forces computed from the 2D model are in per unit length and converted by multiplying the deck length. Generally, wave forces calculated by 2D model are 15 – 20% larger than those by 3D model due to the fully trapped air beneath the deck as mentioned previously. Applying a 3D CFD mode could get more reliable results.

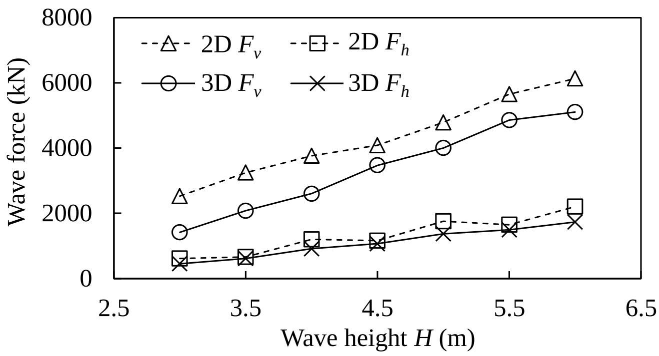

Fig. 4 Comparisons of maximum wave forces between 2D and 3D models

2.4 Characteristics of wave forces

The wave-air-structure interaction simulated in the 3D CFD model for a typical case (D = 12.5 m and H = 3 m) is presented in Fig. 5. In this case, the bridge deck is elevated from the surge water level, and the wave is large enough to exceed the top of the deck. The changing 3D numerical domains are presented in Figs. 5 (a), (c), and (e), respectively, and the corresponding wave profiles in the middle of the deck are shown in Figs. 5 (b), (d), and (f). The three stages include: initial stage before the wave arrives, the water surface starts to rise, and overtopping occurs. The solitary wave progresses along the x axis, from the left side to the right side. The air phase in the upper part of the numerical domain is not shown for a clear illustration. The wave profile is disturbed when the crest reaches the bridge deck as indicated in Fig. 5 (d), and overtopping occurs as the water surface further increases. It is observed in Fig. 5 (f) that there exists a large amount of air trapped in the small cell formed by deck, girders, and diaphragms. The trapped air could significantly increase the total uplift wave forces on the bridge deck, threatening the structural safety.

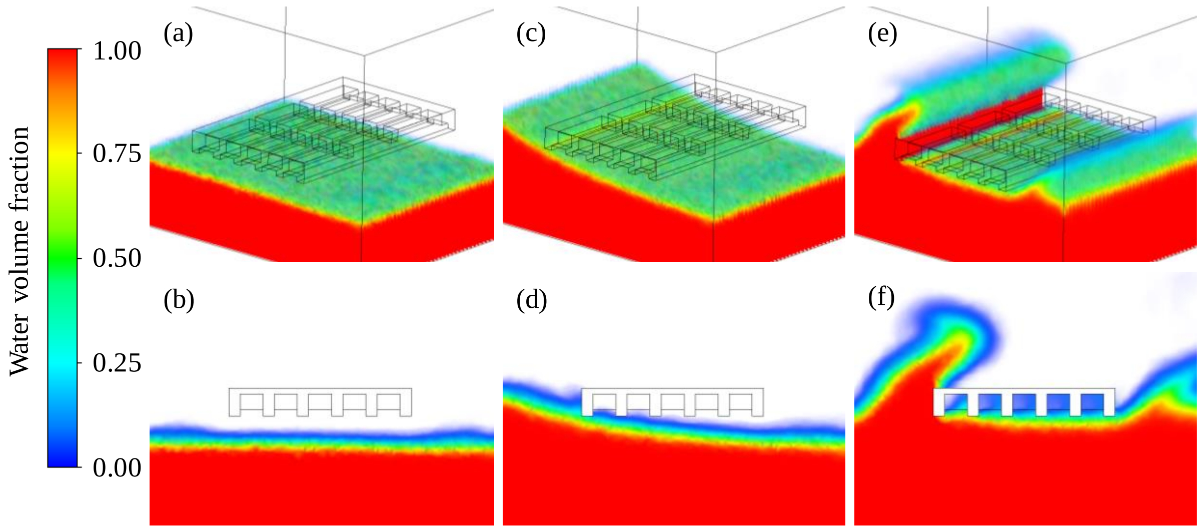

Fig. 5 Simulated wave-air-structure interaction in the 3D numerical model

Fig. 6 shows the peak vertical and horizontal wave forces on the bridge deck during the wave-structure interaction for different surge and wave scenarios. The peak vertical wave force F_v is in a near linear relationship with wave height H, and increases for larger surge water depth D. For small H, F_h has similar value for all the water depths, while for larger H, F_h increases as D increases. Generally, F_v has a much larger magnitude than F_h. The maximum vertical wave force F_v could reach an extreme large value over the self-weight of the bridge span, which is about 2200 kN per span, resulting in deck unseating failure.

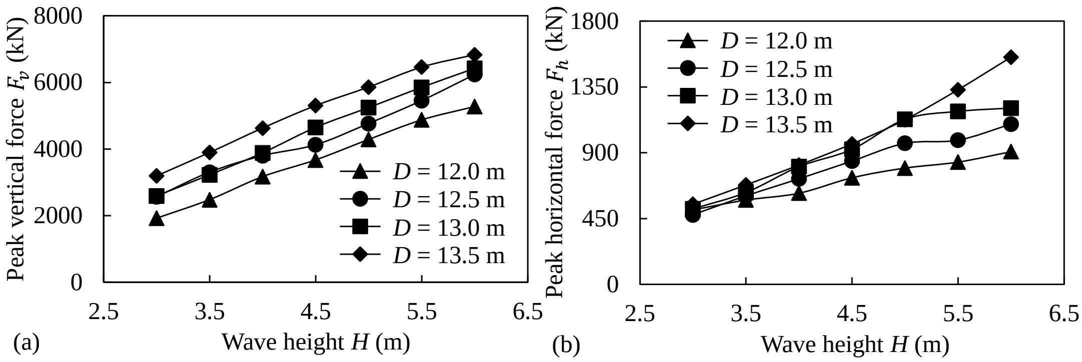

Fig. 6 Peak vertical and horizontal wave forces

2.5 Quantification of the results based on the ANN

The 3D CFD model could provide reliable results as introduced previously but may be limited to its high computational cost. In addition, the wave force on the bridge model is affected by many variables including surge and wave parameters as well as structural dimensions. It could hardly reach an accurate estimation of the wave force by using common analytical methods. For instance, AASHTO (2008) proposed complicated formulas to calculate maximum wave forces; however, the estimated results could also deviate from experimental measurements (Guo et al., 2015), and specific investigations are recommended on different cases (AASHTO 2008). For a more accurate prediction of wave forces under various wave conditions, especially for the probabilistic risk assessment which requires large amount of calculations, Artificial Neural Network (ANN) is adopted as a multivariate regression method to model the correlated results (Demuth et al. 2014).

The general structure of an ANN is shown in Fig. 7, which is comprised of a collection of connected neurons associated with three types of layers: the input layer, the hidden layer(s) and the output layer. The nonlinear relations between the input X and the output Y are modeled through the connections between the neurons. The output of a neuron in a hidden layer is a function of the linear combinations of the outputs from the neurons in the previous layer as

$$Y = k\left(\sum w_i X_i + b\right) \tag{6}$$

where k = activation function considered as the sigmoid function; X_i = outputs from the previous layer; w_i = weight (importance) of each output; and b = bias term.

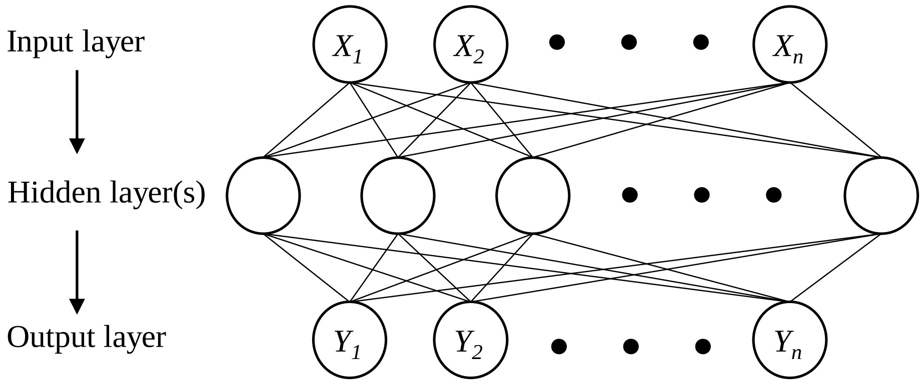

Fig. 7 Schematic of Artificial Neural Network (ANN) structure

ANN model is trained using stochastic gradient descent, which uses randomness to find a good enough set of weights from the inputs to the outputs. To prevent all of weights in the machine learning model from being the same, the network weights are first randomly initialized. A total of 235 samples (i.e. computational wave forces from the 3D model) are calculated. 70% (165) are used to train the neural mode. 15% (35) are used as a validation set, which is employed to determine the termination point of the training process and avoid over fitting. Another 15% (35) is retained to test the model trained from the rest data. Different wave parameters and their interaction effects with each other (i.e., the product of two parameters) are used as inputs to the neural network, including water depth D, wave height H, clearance Z_c, wave celerity c, wave period T, wavelength λ, and wave steepness S. After several calculations and comparisons, 3 hidden layers are adopted in this study, 10 neurons are used in each layer, and the Levenberg-Marquartdt backpropagation algorithm is adopted as the transfer functions. The training results are presented in Fig. 8. As indicated, the output from the ANN model matches the target value (input) well. The Normalized Root-Mean-Square Error (NRMSE) is adopted as the goodness-of-predict, which is calculated as

$$\mathrm{NRMSE} = \frac{\mathrm{RMSE}}{y_{\max} - y_{\min}} = \frac{\sqrt{\sum_{i=1}^{n} \frac{\left(y_i - y_i\right)^2}{n}}}{y_{\max} - y_{\min}} \quad (7)$$

where n = number of the observations; and $\hat{y}$ and y = predicted values and observed values respectively. The ANN model for F_v has small NRMSE value as 0.036, which indicates good training and prediction performance.

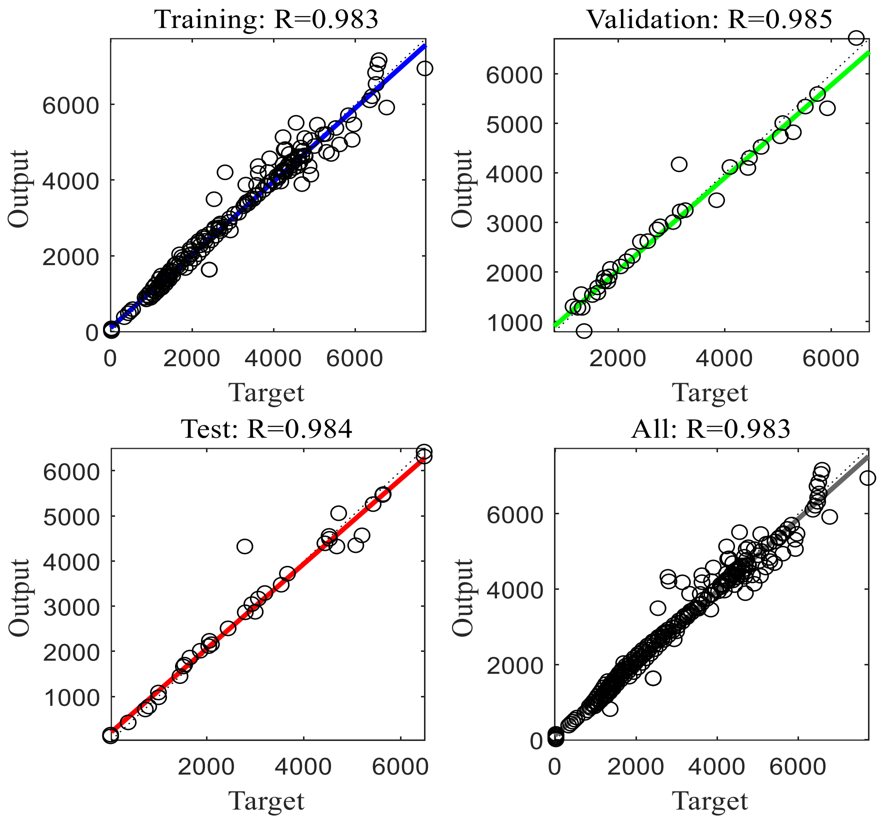

Fig. 8 Training results from Artificial Neural Network (ANN)

3. Bridge reliability analysis under hurricane-induced waves

The 3D CFD model presents the structural responses under hurricane wave intuitively, while the application of this method in practical engineering issue relies on the subsequent vulnerability and reliability analysis. The reliability analysis could assess the structural probabilistic performance during hurricane event by comprehensively considering the structural properties, hazard intensities, and uncertainties associated with demand and capacity. Furthermore, the climate change effects (e.g., amplification in hurricane intensity and occurrence rate) could have significant influence on the long-term structural performance and should be investigated as well. To address all these issues, this section mainly introduces the probabilistic vulnerability model of coastal bridges and the long-term failure risk analysis considering climate change effects.

3.1 Probabilistic vulnerability model and fragility surface

A primary failure mode of coastal bridges subjected to wave forces is deck unseating (Ataei & Padgett 2013). Once the external wave loads on the bridge superstructure exceeds the capacity (or resistance), the limit state reaches, and deck failure occurs. The general function of the vulnerability model is given as

$$P(F) = P\left[G(C_v, D_v) \le 0 \text{ or } G(C_h, D_h) \le 0 \middle| IM\right] \tag{8}$$

where $P(F)$ = probability of deck unseating failure; G = limit state function; C = structural capacity; D = structural demand; IM = hurricane hazard intensity measure; and the subscript v and h account for wave effects in vertical and horizontal directions, respectively. The structural demand, *i.e.* the maximum vertical and horizontal wave loads on the bridge deck, could be derived from the ANN prediction model as mentioned previously. The vertical structural capacity consists of the dead weight of the bridge span as well as the connection strength between the bridge superstructure and substructure (Ataei & Padgett 2013). The horizontal capacity is mainly provided by connections and the friction between the bridge deck and bent. The static weight of the bridge span W_s can be calculated as

$$W_s = \left(d_b W + A_g n_g\right)\gamma l \tag{9}$$

where W = the deck width; A_g = cross-sectional area of girders; n_g = girder numbers; γ = unit weight of the material; and l = span length. The friction between the bridge deck and bent F_f is calculated as

$$F_f = \left(W_s - F_v\right)\mu \tag{10}$$

where μ = coefficient of friction between concrete surfaces taken as 0.6 (ACI 2008). Note that F_f is only considered when $W_s > F_v$. The flip-bolt connection strength can be estimated by the concrete spalling strength as (Ataei & Padgett 2013; Yuan et al. 2018)

$$N_{cb} = \frac{A_N}{A_{N0}} \psi_2 \psi_3 N_b \tag{11}$$

where N_{cb} = the concrete breakout strength; A_N = projected area of the failure surface for the anchor; A_{N0} = projected area of the failure surface of a single anchor remote from edges; N_b = the basic concrete breakout strength of a single anchor; and ψ_2 and ψ_3 = modification factors. Based on previous investigations on connection strength (Robertson et al. 2011; Yuan et al. 2018), the vertical capacity provided by each flip-bolt connection is about 44 kN, while horizontal capacity is 96 kN on average.

The numerical and analytical methods provide deterministic results for structural demand and capacity, which may deviate from real values because of the uncertainties associated with structural demand and capacity. For instance, the concrete density could be slightly different from the standard values, and its strength would also be different. Thus, the probabilistic distributions of demand and capacity variables are considered in the reliability analysis and introduced in this section. A Weibull-generalized Pareto (WGP) model (Wu et al. 2016) is employed to model the wave height distribution in coastal shallow water as

$$f_W(h) = \frac{\kappa\varphi}{\rho H_s}\left(\frac{h}{\rho H_s}\right)^{\kappa-1} \exp\left[-\varphi\left(\frac{h}{\rho H_s}\right)^{\kappa}\right] \qquad h \le H_s \tag{12}$$

$$\kappa = 2\left(1-\omega\left(\frac{H_s}{D}\right)^{1.7}\right)^{-1} \tag{13}$$

$$f_{GP}(h) = \frac{1}{\alpha\rho H_s}\left(1+\frac{\xi}{\alpha}\frac{(h-\rho H_s)}{\rho H_s}\right)^{-\frac{1}{\xi}-1} \qquad h > H_s \tag{14}$$

$$\xi = \alpha\left(1-2\beta\pi\frac{\tanh(k_L D)}{k_L \rho H_s}\right)^{-1} \tag{15}$$

where φ = scale parameter of the Weibull distribution taken as 5; H_s = significant wave height; ω = Weibull shape adjustment coefficient taken as 1; k_L = wave number; α = GP scale parameter taken as 0.22; β = Miche limit coefficient taken as 0.15 (Miche 1944); and ρ = estimation factor taken as 1 (Wu et al. 2016). The surge height distribution during a hurricane is hard to predict due to the complex meteorological environment. Several investigations tried to predict the surge height distribution, but lack of data support due to difficult field measurement. Hence, a uniform distribution ranging ± 20% is utilized for the surge height (Saeidpour et al. 2019).

With respect to the structural capacity, uncertainties in the unit weight of construction materials, workmanship error and construction error are considered in the capacity modeling. A normal distribution for concrete and steel density is used in this study according to JCSS (2006). The mean density for reinforced concrete is 2,400 kg/m^3 and the coefficient of variation (COV) is 0.04. For steel, the mean density is 7,850 kg/m^3 and COV is 0.01. A uniform distribution with lower and upper limits of 95 and 105% is used to account for workmanship and construction errors in deck thickness. Additionally, a model error ε accounting for the concrete strength uncertainties with a mean of 1 and COV of 0.23 (Eligehausen et al. 2006) is applied when calculating N_{cb}. Table 1 lists parameters with respect to demand and capacity modeling, where μ is the mean value and σ is the standard deviation.

Table. 1 Parameters required for demand and capacity calculation

Structural parameters		
Deck thickness d_b	Uniform	95%~105%
Concrete density γ_c	Normal	μ = 2400, σ = 96
Steel density γ_s	Normal	μ = 7850, σ = 78.5
Concrete breakout strength N_b	Normal	μ = 176, σ = 40.48
Breakout model error ε	Normal	μ = 1, σ = 0.23
Wave parameters		
Wave height H	WGP distribution	
Surge height S	Uniform distribution	± 20%
Surge water depth D	Initial water depth plus surge height	

Furthermore, the bridge failure probability under certain intensity hurricane could be assessed by tracing the correlation between wave properties with hurricane intensity. The significant wave height is determined by the maximum hurricane wind speed as (CERC, 1984)

$$H_s = 5.112 \times 10^{-4} U_A F^{1/2} \tag{16}$$

$$U_A = 0.71 U_{\max}^{1.23} \tag{17}$$

where U_A = wind-stress factor; F = fetch length, which is treated deterministically as 1 km; and $U_{\max}$ = maximum hurricane wind speed. The surge height S is assumed as a linear function with $U_{\max}$ (Liang & Julius 2011).

With the probabilistic vulnerability model introduced above, the bridge fragility probability under given *IM*(s) could be assessed. Fig 9 (a) presents the fragility surface generated for different surge and wave scenarios. As illustrated, the bridge failure probability sharply increases with larger D and H_s. P is more sensitive to the value of D than H_s, which indicates increasing the relative distance from the deck to water level could be an effective retrofit. Additionally, the fragility curve derived for various hurricane intensities is plotted as Fig. 9 (b). Hurricane categories based on the Saffir-Simpson Hurricane Wind Scale (SSHWS) are highlighted as well. It is observed that the bridge is under relatively small failure risk under a category 2 or 3 hurricane, while sharply increases for hurricane above category 4.

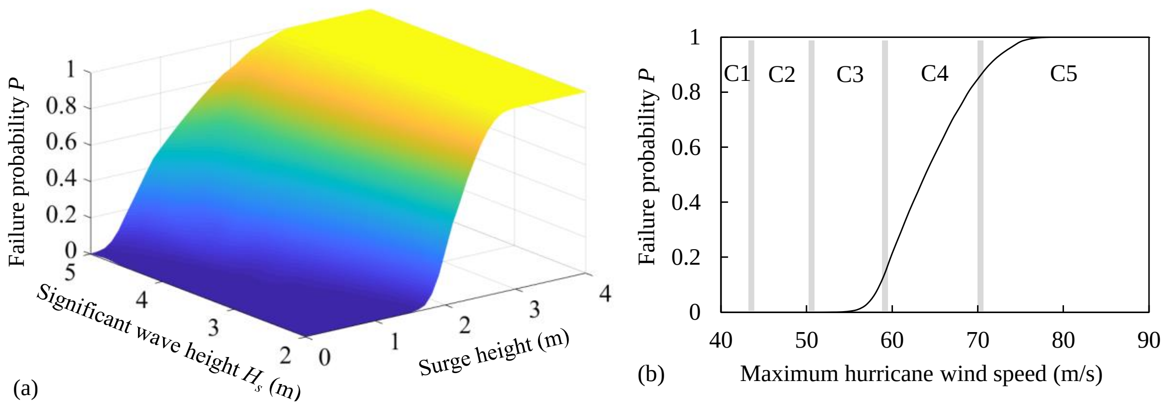

Fig. 9 (a) Bridge fragility surface and (b) bridge failure risk versus maximum hurricane wind speed

3.2 Hurricane hazard model and climate change effects

The long-term failure risk refers to the bridge failure probability under hurricane wave impacts during its service life, which could be assessed by accumulating the product of hazard occurrence rate and the corresponding bridge failure probability under the investigated hazard scenario. Combining the fragility surface with appropriate hurricane occurrence model, as well as the climate change effects, the long-term bridge failure risk during the service life could be assessed, which expedites management and maintenance.

Several studies utilized annual wind speed distribution over an area as the hurricane occurrence model (Batts et al. 1980; Peterka & Shahid 1998), but such method may underestimate the duration when the hurricane wind speed is zero (i.e., hurricane does not occur). Recognizing this, the method of utilizing the probability distribution of the maximum wind speed during a hurricane event to describe the hurricane risk (Li et al., 2016) is adopted in this study. Li et al., (2016) summarized a two parameter Weibull distribution for the maximum hurricane wind speed by collecting historical hurricane data record (for a period over 100 years) from the US National Hurricane Center's Database. Additionally, a Poisson point process model is utilized to calculate hurricane occurrence rate. The cumulative density function (CDF) of the maximum wind speed during hurricane events F_U, and the CDF of maximum wind speed during [0, T] period F_r in this method are given by

$$F_U(u) = 1 - \exp\left[-\left(\frac{u}{\alpha}\right)^{\beta}\right] \tag{18}$$

$$F_r(u) = \exp\left[-\omega T\left(1 - F_U(u)\right)\right] \tag{19}$$

where u = wind speed; α and β = parameters sorted from the weather record data; T = duration in year; and ω = mean annual occurrence rate of the hurricane.

Furthermore, to describe the long-term climate change effects including the amplification in hurricane occurrence rate and intensity, the ω and α are treated time-variant as $\omega(t)$, $\alpha(t)$, while the scale parameter β is assumed unchanged as (Bjarnadottir et al. 2011)

$$\omega(t) = \omega_0 + r_\omega t \tag{20}$$

$$\alpha(t) = \alpha_0 + r_\alpha t \tag{21}$$

where r_ω and r_a = annual increment rate in hurricane occurrence rate and maximum wind speed. Based on previous research on climate change effects (Knutson et al. 2010), r_ω and r_a are taken as 4.9×10^{-4} and 0.0718, respectively, which corresponds to a 10% increase in 50 years. The relative parameter ω_0, α_0, and β are determined as 0.245, 35.9, and 2.06, respectively based on historical hurricanes record of Miami-Dade region obtained from the US National Hurricane Center's Database (Li et al., 2016).

Comparisons of climate change (CM) effects on the maximum hurricane wind speed during 20-year, 50-year, and 100-year assessment periods are presented in Fig. 10. It is apparent that the $U_{\max}$ is significantly increased in all the cases. Correspondingly, the bridge failure risks without considering CM effects are 0.1806, 0.3825, and 0.5991, while once with CM effects included, these values enlarge to 0.2306, 0.5938, 0.9264, respectively.

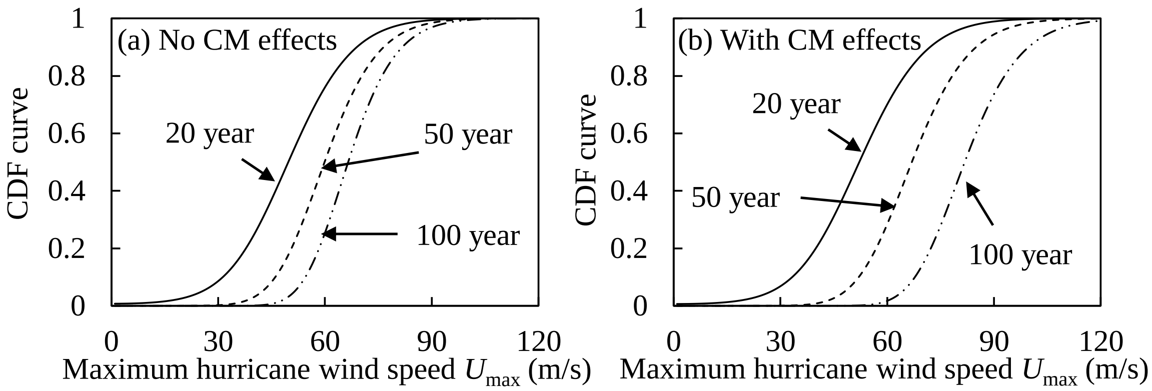

Fig. 10 Cumulative distribution function (CDF) of maximum hurricane wind speed with and without considering Climate Change (CM) effects

4. Evaluation and comparison of different retrofit actions

The performance and reliability investigations reveal high potential risk of bridge failure subjected to wave forces during a hurricane event. Such vulnerable bridges threaten public's life and property severely and retrofitting techniques could be a solution to this problem. In this section, effects of different retrofits in reducing the bridge failure risk are examined and compared. The investigated retrofit actions include inserting air venting holes, enhancing connection strength, and elevating bridge structure.

4.1 Inserting air venting holes

Air entrapment is an integral part of the total wave load on a coastal bridge deck. The presence of air pockets between the water surface and bridge deck can result in an increase of the effective volume of the deck and an increase in the buoyancy force. Through the laboratory experiments, El Ghamry, (1963) found that the formation of the air entrapment underneath the deck can result in ten times larger uplift forces. Cuomo et al., (2009) conducted laboratory experiments on a 1:10 scale bridge deck to examining the effects of air venting hole. It was shown that the air venting hole could significantly reduce the total pressure on the bridge deck. McPherson, (2010) discussed the hydrostatic effect of the trapped air and pointed out a more sufficient model for the wave-air-structure interaction is required.

Thus, a 3D CFD model is established in this study to investigate the effects of air venting hole on reducing the total wave loads for the investigated bridge. Considering the cored holes could affect the structural capacity, a conservative venting ratio of 3% (hole area over the deck area) is adopted in this study. It should be noted that although the component of trapped air would decrease in this case, the trapped air could not be fully released. The 3D bridge model with inserted holes is presented in Fig. 11, and other numerical model setups are similar to those introduced previously.

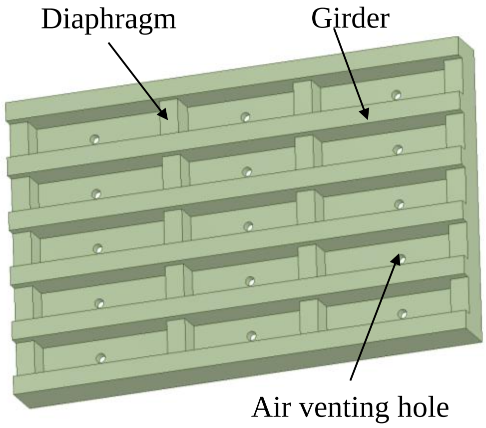

Fig. 11 3D bridge model with air venting holes

Comparisons of peak vertical and horizontal wave forces on bridge deck with and without air venting holes are presented in Fig. 12. Four different surge water depths are shown including D = 12.5, 13.0, 13.5, and 14.0 m. It is observed that inserting air holes could reduce the peak vertical wave force F_v for 10 – 20% for the investigated cases. However, the peak horizontal force F_h slightly increases, which may be attribute to the following reasons: (1) air venting hole decreases the F_v forcing area (lateral surface), but increases the F_h forcing area (vertical surface); (2) the escaped trapped air could cause hydrodynamic influence on the bridge deck; and (3) the air venting hole disturbs the solitary wave profile and changes the wave force property. Similarly, F_v is modeled by ANN for the subsequent reliability analysis.

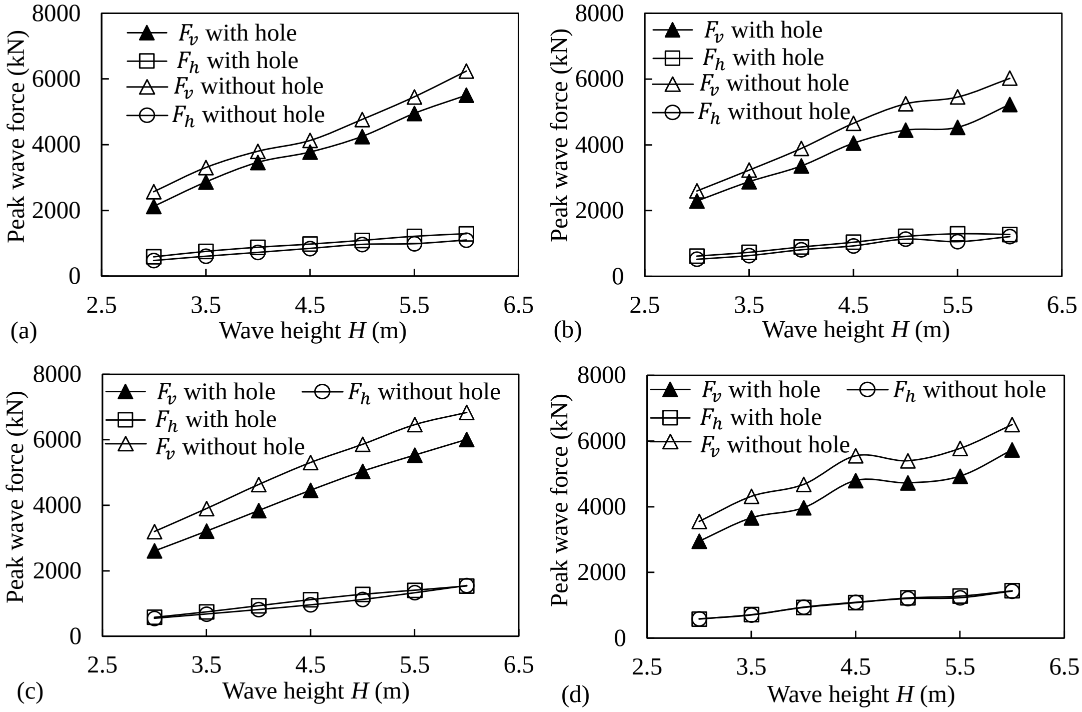

Fig. 12 Comparisons of peak wave forces on bridge deck with and without air venting holes

4.2 Enhancing connection strength

The idea of using existing seismic retrofitting techniques for simply supported bridges as a solution to surge and wave problem has been proposed recently (Okeil & Cai 2008). The deck unseating risk could be reduced by enhancing the connection strength between bridge superstructure and substructure. Typical ways to stiffen the connection strength are through flip-bolt connections or joint restrainers as shown in Fig. 13. These methods are designed to limit the relative displacement at the expansion joints when the original joint design does not prevent loss of support. While pounding may still occur at the joint, these methods could prevent unseating of the bridge deck and total damage of the structure.

The capacity of a flip-bolt connection could be determined by the concrete spalling strength, and that for the joint restrainer is estimated by tensile capacity of cables. There is a limit on the number of the constraints considering the drilling or coring of the existing concrete structure is required. Based on previous research on connection strength (Robertson et al. 2011; Yuan et al. 2018), the average vertical capacity from each flip-bolt connection is about 44 kN, *i.e.*, 4 connections installed on the two ends of a girder could provide a total of 176 kN vertical capacity. Considering the deck is only constrained at the seaward and landward bearings in the original design, the retrofit action is to add connections on the remaining four girders as Fig. 13 (a). Thus, the additional connection strength is about 44 × 4 × 4 = 704 kN.

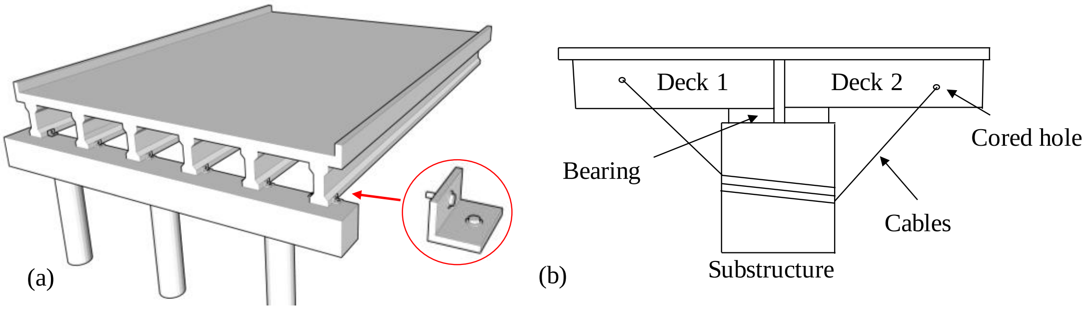

Fig. 13 (a) Flip-bolt connections and (b) typical joint restrainers

4.3 Elevating bridge structure

Since the uplift wave force is significantly influenced by the relative distance from the deck to the water level, elevating the structure could be one of the most effective ways to reduce the wave loads, which is widely adopted in post-disaster reconstruction. In this study, this method is investigated as well, and the bridge deck is assumed to be lifted by 0.5 m. The numerical modeling and reliability analysis can be conducted accordingly.

4.4 Comparisons of different retrofit methods

The fragility curves generated for the bridge deck improved by different retrofit actions are plotted in Fig. 14. As illustrated, 3% air venting hole decreases F_v by 10 - 20%, and similar effect is observed in reducing bridge failure probability. Enhancing connection strength has a better improvement effect for all the hurricane scenarios as compared with inserting air venting holes, and larger elevation has better retrofitting effects. Elevating bridge structure has a best performance among all the three methods, especially to resist large scale hurricane.

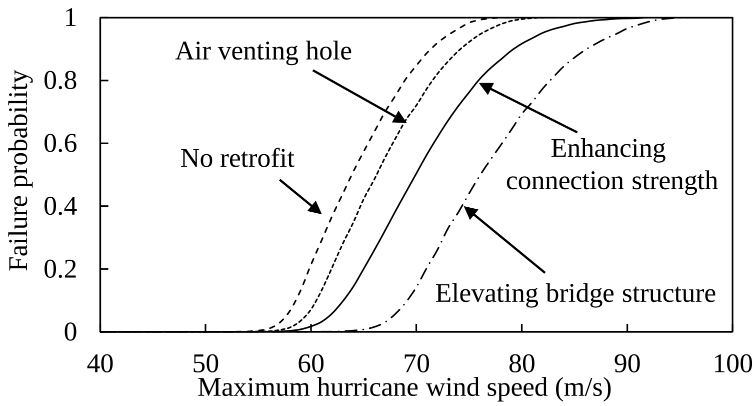

Fig. 14 Comparison of bridge failure probabilities with different retrofits

The bridge long-term failure risks with different retrofits are listed in Table. 2. As indicated, elevating bridge structure is the most effective retrofit method in reducing the long-term failure risk. The failure probabilities for investigated time periods 20-, 50- and 100-year with considering CM effects are 0.0759, 0.2655, and 0.6584, respectively. Influence of inserting air venting hole is limited when considering the uncertainties associated with hurricane hazard model and climate change effects. It should be noted that enhancing connection strength has similar effects with elevating bridge structure during a short-term period (0.1402 and 0.1909 for 20 year), which means that it could be utilized as an effective emergency measure. Generally, neglecting the climate change effects could result in an underestimation of long-term bridge failure risk by 10 – 20 %.

Table. 2 Bridge long-term failure risk under different scenarios

Retrofits		No retrofit	IAVH	ECS	EBS
With CM effects	20 year	0.2306	0.1909	0.1402	0.0759
	50 year	0.5938	0.5246	0.4196	0.2655
	100 year	0.9264	0.8921	0.8145	0.6584
No CM effects	20 year	0.1806	0.1465	0.1045	0.0533
	50 year	0.3825	0.3188	0.2345	0.1256
	100 year	0.5991	0.5180	0.3981	0.2288

Note: CM means Climate Change; IAVH means Inserting Air Venting Holes; ECS means Enhancing Connection Strength; and EBS means Elevating Bridge Structure.

5. Conclusions

This study focuses on reliability-based retrofit assessment of coastal bridges subjected to extreme wave forces and proposes a systematic analysis framework using the 3D CFD model and ANN method. The established 3D CFD model could simulate the extreme solitary wave, as well as the complex wave-structure interaction. The wave-induced forces are investigated and quantified with multiple surge and wave parameters by ANN model. According to the numerical and machine learning results, bridge fragility curve is plotted comprehensively considering the uncertainties involved in capacity, demand, and hurricane hazard. Given climate change effects (e.g., increment in hurricane occurrence rate and amplification of intensity), long-term failure risk is assessed.

Three retrofit measures are examined: inserting air venting holes, enhancing connection strength, and elevating bridge structure. An additional 3D numerical model for the bridge deck inserted with air venting holes is established to explore the effects of trapped air and air holes. Their effects in improving structural performance and reducing bridge failure risk are compared.

The conclusions are as follows:

1. The 3D CFD model reveals that the extreme wave force on the bridge deck could reach over 5000 kN per span, much larger than the static weight of the deck (about 2500 kN). The deck could be easily uplifted and then washed away by lateral wave force.
2. The original bridge is inadequately designed to resist hurricane surge and waves, especially under the climate change scenarios. The bridge failure risk reaches 0.2306, 0.5938, and 0.9264 for a 20-, 50-, and 100-year evaluation duration, respectively.
3. A 3% venting ratio air holes could reduce the peak vertical wave force by 10% - 20%, but the peak horizontal wave force increases, which may lead to problem of overturning and structural vibration.
4. Enhancing connection strength between the bridge superstructure and substructure could be an effective method in reducing the bridge failure risk when comprehensively considering uncertainties and climate change effects.

5. Climate change effects have significant influence on bridge reliability, especially for those with long-term service life. The long-term failure risk could increase by about 0.05 during a 20-year service life, while for a 100-year period, the amplification could reach over 0.15.

The evaluation and comparison of different retrofit methods in this study could help guide future engineering practice for bridges in coastal regions. Other bridge types should be considered, effects of overturning moment, and updating climate change model developing with meteorological research should be considered in future study.

References

AASHTO. (2008). *Guide specifications for bridges vulnerable to coastal storms* (p. 55).

Akiyama, M., Frangopol, D. M., Arai, M., & Koshimura, S. (2012). Probabilistic assessment of structural performance of bridges under tsunami hazard. *Structures Congress 2012 - Proceedings of the 2012 Structures Congress*, 1919–1928.

Ataei, N., & Padgett, J. E. (2013). Probabilistic modeling of bridge deck unseating during hurricane events. *Journal of Bridge Engineering*, *18*(4), 275–286.

Azadbakht, M., & Yim, S. C. (2016). Effect of trapped air on wave forces on coastal bridge superstructures. *Journal of Ocean Engineering and Marine Energy*, *2*(2), 139–158.

Batts, M. E., Cordes, M. R., Russell, L. R., Shaver, J. R., & Simin, E. (1980). Hurricane wind speeds in the United States. *Journal of the Structural Division*, *106*(10), 2001–2016.

Bender, M. A., Knutson, T. R., Tuleya, R. E., Sirutis, J. J., Vecchi, G. A., Garner, S. T., & Held, I. M. (2010). Modeled impact of anthropogenic warming on the frequency of intense Atlantic hurricanes. *Science*, *327*(5964), 454–458.

Biondini, F., & Frangopol, D. M. (2016). Life-cycle performance of deteriorating structural systems under uncertainty: Review. *Journal of Structural Engineering (United States), 142*(9), F4016001.

Bjarnadottir, S., Li, Y., & Stewart, M. G. (2011). A probabilistic-based framework for impact and adaptation assessment of climate change on hurricane damage risks and costs.

Structural Safety, *33*(3), 173–185.

Bozorgnia, M., & Lee, J. J. (2012). Computational fluid dynamic analysis of highway bridges exposed to hurricane waves. *Proceedings of the Coastal Engineering Conference*, 1–14.

Bradner, C., Schumacher, T., Cox, D., & Higgins, C. (2011). Experimental setup for a large-scale bridge superstructure model subjected to waves. *Journal of Waterway, Port, Coastal and Ocean Engineering*, *137*(1), 3–11.

BRICKER, J. (2011). CFD Analysis of Bridge Deck Failure due to Tsunami. *Proceedings of the …*, *September*, 1398–1409.

Bricker, J. D., & Nakayama, A. (2014). Contribution of trapped air, deck superelevation, and nearby structures to bridge deck failure during a tsunami. *Journal of Hydraulic Engineering*, *140*(5).

C. E. R. C. (1984). *Shore Protection Manual*. Department of the Army, Waterways Experiment Station, Corps of Engineers.

Cuomo, G., Shimosako, K. ichiro, & Takahashi, S. (2009). Wave-in-deck loads on coastal bridges and the role of air. In *Coastal Engineering* (Vol. 56, Issue 8, pp. 793–809). World Scientific.

Demuth, H. B., Beale, M. H., De Jess, O., & Hagan, M. T. (2014). *Neural network design*. Martin Hagan.

Dong, Y., & Frangopol, D. M. (2016). Probabilistic Time-Dependent Multihazard Life-Cycle Assessment and Resilience of Bridges Considering Climate Change. *Journal of Performance of Constructed Facilities*, *30*(5).

Dong, Y., & Frangopol, D. M. (2017). Probabilistic life-cycle cost-benefit analysis of portfolios of buildings under flood hazard. *Engineering Structures*, *142*, 290–299.

Douglass, S. L., Hughes, S. a, Rogers, S., & Chen, Q. (2004). The Impact of Hurricane Ivan on the Coastal Roads of Florida and Alabama: A Preliminary Report. *Rep. to Coastal Transportation Engineering Research and Education Center, Univ. of South Alabama, Mobile, Ala*, 1–19.

El Ghamry, O. A. (1963). *Wave forces on a dock*.

Eligehausen, R., Mallée, R., & Silva, J. F. (2006). *Anchorage in concrete construction* (Vol. 10). John Wiley & Sons.

Elsner, J. B., Kossin, J. P., & Jagger, T. H. (2008). The increasing intensity of the strongest tropical cyclones. *Nature*, *455*(7209), 92–95.

Guo, A., Fang, Q., Bai, X., & Li, H. (2015). Hydrodynamic Experiment of the Wave Force Acting on the Superstructures of Coastal Bridges. *Journal of Bridge Engineering*, *20*(12), 1–11.

Guo, A., Li, H., Ba, X., Guan, X., & Li, H. (2015). Experimental investigation on the cyclic performance of reinforced concrete piers with chloride-induced corrosion in marine environment. *Engineering Structures*, *105*, 1–11.

Guo, X., & Chen, Z. (2016). Lifecycle multihazard framework for assessing flood scour and earthquake effects on bridge failure. *ASCE-ASME Journal of Risk and Uncertainty in Engineering Systems, Part A: Civil Engineering*, *2*(2), C4015004.

Hayatdavoodi, M., & Ertekin, R. C. (2016). Review of wave loads on coastal bridge decks. *Applied Mechanics Reviews*, *68*(3).

Hayatdavoodi, M., Seiffert, B., & Ertekin, R. C. (2014a). Experiments and computations of solitary-wave forces on a coastal-bridge deck. Part II: Deck with girders. *Coastal Engineering*, *88*, 210–228.

Hayatdavoodi, M., Seiffert, B., & Ertekin, R. C. (2014b). Experiments and computations of solitary-wave forces on a coastal-bridge deck. Part II: Deck with girders. *Coastal Engineering*, *88*, 210–228.

Huang, W., & Xiao, H. (2009). Numerical modeling of dynamic wave force acting on Escambia bay bridge deck during Hurricane Ivan. *Journal of Waterway, Port, Coastal and Ocean Engineering*, *135*(4), 164–175.

Istrati, D., & Buckle, I. (2019). Role of trapped air on the tsunami-induced transient loads and response of coastal bridges. *Geosciences (Switzerland)*, *9*(4).

JCSS. (2006). JCSS PROBABILISTIC MODEL CODE Part 3: RESISTANCE MODELS. In *Lancet*.

Jin, J., & Meng, B. (2011). Computation of wave loads on the superstructures of coastal highway bridges. *Ocean Engineering*, *38*(17–18), 2185–2200.

Khelifa, A., Garrow, L. A., Higgins, M. J., & Meyer, M. D. (2013). Impacts of climate change on scour-vulnerable bridges: Assessment based on HYRISK. *Journal of Infrastructure Systems*, *19*(2), 138–146.

Knutson, T. R., McBride, J. L., Chan, J., Emanuel, K., Holland, G., Landsea, C., Held, I., Kossin, J. P., Srivastava, A. K., & Sugi, M. (2010). Tropical cyclones and climate change. *Nature Geoscience*, *3*(3), 157–163.

Lehrman, J. B., Higgins, C., & Cox, D. (2012). Performance of highway bridge girder anchorages under simulated hurricane wave induced loads. *Journal of Bridge Engineering*, *17*(2), 259–271.

Li, Q., Wang, C., & Zhang, H. (2016). A probabilistic framework for hurricane damage assessment considering non-stationarity and correlation in hurricane actions. *Structural Safety*, *59*, 108–117.

Li, Y., Dong, Y., Frangopol, D. M., & Gautam, D. (2020). Long-term resilience and loss assessment of highway bridges under multiple natural hazards. *Structure and Infrastructure Engineering*, *16*(4), 626–641.

Liang, M. S., & Julius, S. (2011). On the Coastal Topography and Storm Surge for Infrastructure Risk Assessment and Adaptation. *World Environmental and Water Resources Congress 2017*, 232–240.

Madsen, P. A., Fuhrman, D. R., & Schäffer, H. A. (2008). On the solitary wave paradigm for tsunamis. *Journal of Geophysical Research: Oceans*, *113*(12).

Matemu, C., Crowley, R., & Resio, D. (2020). Development of a one-way coupled diffraction/trapped air model for predicting wave loading on bridges under water wave attack. *Journal of Fluids and Structures*, *97*, 103067.

McPherson, R. L. (2010). *Hurricane induced wave and surge forces on bridge decks*. Texas A & M University.

Moftakhari, H. R., Salvadori, G., AghaKouchak, A., Sanders, B. F., & Matthew, R. A. (2017).

Compounding effects of sea level rise and fluvial flooding. *Proceedings of the National Academy of Sciences*, *114*(37), 9785–9790.

Mondoro, A., Frangopol, D. M., & Soliman, M. (2017). Optimal risk-based management of coastal bridges vulnerable to hurricanes. *Journal of Infrastructure Systems*, *23*(3).

Motley, M. R., Wong, H. K., Qin, X., Winter, A. O., & Eberhard, M. O. (2016). Tsunami-induced forces on skewed bridges. *Journal of Waterway, Port, Coastal and Ocean Engineering*, *142*(3), 1–12.

MUNK, W. H. (1949). the Solitary Wave Theory and Its Application To Surf Problems. *Annals of the New York Academy of Sciences*, *51*(3), 376–424.

NYCDEP. (2008). *Climate change program, Assessment and action plan*.

Okeil, A. M., & Cai, C. S. (2008). Survey of short- and medium-span bridge damage induced by Hurricane Katrina. *Journal of Bridge Engineering*, *13*(4), 377–387.

Padgett, J., Desroches, R., Nielson, B., Yashinsky, M., Kwon, O. S., Burdette, N., & Tavera, E. (2008). Bridge damage and repair costs from Hurricane Katrina. *Journal of Bridge Engineering*, *13*(1), 6–14.

Peterka, J. A., & Shahid, S. (1998). Design gust wind speeds in the United States. *Journal of Structural Engineering*, *124*(2), 207–214.

Qin, J. (2012). *Probabilistic analysis of large-scale engineering systems* [ETH Zurich].

Qin, J. (2018). Information-dependent seismic reliability assessment of bridge networks based on a correlation model. *Engineering Structures*, *176*, 314–323.

Qin, J., & Faber, M. H. (2012). Risk Management of Large RC Structures within Spatial Information System. *Computer-Aided Civil and Infrastructure Engineering*, *27*(6), 385–405.

Robertson, I. N., Riggs, R. H., Yim, S. C. S., & Young, Y. L. (2007). Lessons from Hurricane Katrina storm surge on bridges and buildings. *Journal of Waterway, Port, Coastal and Ocean Engineering*, *133*(6), 463–483.

Robertson, I. N., Yim, S., & Tran, T. (2011). Case study of concrete bridge subjected to hurricane storm surge and wave action. *Solutions to Coastal Disasters 2011 - Proceedings* *of the 2011 Solutions to Coastal Disasters Conference*, 728–739.

Robertsson, J. O. A., & Blanch, J. O. (2020). *Numerical Methods, Finite Difference* (pp. 1–9).

Rosenzweig, C., Solecki, W. D., Blake, R., Bowman, M., Faris, C., Gornitz, V., Horton, R., Jacob, K., LeBlanc, A., Leichenko, R., & others. (2011). Developing coastal adaptation to climate change in the New York City infrastructure-shed: process, approach, tools, and strategies. *Climatic Change*, *106*(1), 93–127.

Saeidpour, A., Chorzepa, M. G., Christian, J., & Durham, S. (2019). Probabilistic hurricane risk analysis of coastal bridges incorporating extreme wave statistics. *Engineering Structures*, *182*(June 2018), 379–390.

Sarpkaya, T., & Isaacson, M. (1981). *Mechanics of wave forces on offshore structures.*

Sawyer, A. (2008). *Determination of hurricane surge wave forces on bridge superstructures and design/retrofit options to mitigate or sustain these forces*.

Seiffert, B., Hayatdavoodi, M., & Ertekin, R. C. (2014). Experiments and computations of solitary-wave forces on a coastal-bridge deck. Part I: Flat Plate. *Coastal Engineering*, *88*, 194–209.

Seiffert, B. R. (2014). *Tsunami and Storm Wave Impacts on Coastal Bridges*. 201 pp.

Steffler, P. (1999). Hydraulics of open channel flow. In *Journal of Hydraulic Engineering* (Vol. 125, Issue 11). Elsevier.

Veritas, N. (2000). *Environmental conditions and environmental loads*. Det Norske Veritas.

Wu, Y., Randell, D., Christou, M., Ewans, K., & Jonathan, P. (2016). On the distribution of wave height in shallow water. *Coastal Engineering*, *111*, 39–49.

Xiao, H., Huang, W., & Chen, Q. (2010). Effects of submersion depth on wave uplift force acting on Biloxi Bay Bridge decks during Hurricane Katrina. *Computers & Fluids*, *39*(8), 1390–1400.

Xu, G., Cai, C., & Deng, L. (2017). Numerical prediction of solitary wave forces on a typical coastal bridge deck with girders. *Structure and Infrastructure Engineering*, *13*(2), 254–272.

Xu, G., & Cai, C. S. (2017). Numerical investigation of the lateral restraining stiffness effect on the bridge deck-wave interaction under Stokes waves. *Engineering Structures*, *130*, 112–123.

Xu, G., Cai, C. S., & Chen, Q. (2017). Countermeasure of air venting holes in the bridge deck--wave interaction under solitary waves. *Journal of Performance of Constructed Facilities*, *31*(1), 4016071.

Xu, G., Cai, C. S., & Han, Y. (2016). Investigating the characteristics of the solitary wave-induced forces on coastal twin bridge decks. *Journal of Performance of Constructed Facilities*, *30*(4), 4015076.

Yuan, P., Xu, G., Chen, Q., & Cai, C. S. (2018). Framework of Practical Performance Evaluation and Concept of Interface Design for Bridge Deck-Wave Interaction. *Journal of Bridge Engineering*, *23*(7), 1–12.

Zhang, J., Zheng, J., Jeng, D. S., & Guo, Y. (2015). Numerical simulation of solitary-wave propagation over a steady current. *Journal of Waterway, Port, Coastal and Ocean Engineering*, *141*(3).

Zheng, Y., & Dong, Y. (2019). Performance-based assessment of bridges with steel-SMA reinforced piers in a life-cycle context by numerical approach. *Bulletin of Earthquake Engineering*, *17*(3), 1667–1688.

Zheng, Y., Dong, Y., & Li, Y. (2018). Resilience and life-cycle performance of smart bridges with shape memory alloy (SMA)-cable-based bearings. *Construction and Building Materials*, *158*, 389–400.

Zhu, D., & Dong, Y. (2020). Experimental and 3D numerical investigation of solitary wave forces on coastal bridges. *Ocean Engineering*, *209*, 107499.